



ORIGINAL ARTICLE

Photoresponsive oxidase-like phosphorescent carbon dots in colorimetric Hg^{2+} detection



Xiaojie Sun^a, Shiqing Luo^a, Lifang Zhang^{a,c,*}, Yanming Miao^{b,*}, Guiqin Yan^b

^a School of Chemistry and Materials Science, Shanxi Normal University, Taiyuan 030006, China

^b School of Life Science, Shanxi Normal University, Taiyuan 030006, China

^c Research Institute of Materials Science of Shanxi Normal University & Collaborative Innovation Center for Shanxi Advanced Permanent Magnetic Materials and Technology, Taiyuan 030006, China

Received 1 October 2022; accepted 10 January 2023

Available online 26 January 2023

KEYWORDS

Long-life room-temperature phosphorescent;
Nitrogen-doped carbon dots;
Photoresponsive;
Oxidase mimic;
Colorimetric;
 Hg^{2+} detection

Abstract Developing novel photoresponsive oxidase mimics is highly useful for environmental pollution monitoring and biological sensing. Herein, long-life room-temperature phosphorescent nitrogen-doped carbon quantum dots (P-NCDs) were synthesized from triethylenetetramine hexaacetic acid via a simple one-step hydrothermal method. The P-NCDs showed high photoresponsive oxidase-like activity. On this basis, a P-NCD-based photostimulated colorimetric sensing system was developed and used to detect Hg^{2+} in environmental and biological samples. P-NCDs under 365 nm UV lamp irradiation converted dissolved oxygen, via triplet excited state (T_1) exciton transfer, to singlet oxygen ($^1\text{O}_2$), which then oxidized 3,3',5,5'-tetramethylbenzidine (TMB), leading to a color changing reaction. Cysteine can suppress the catalysis of P-NCDs, and its specific complexation with Hg^{2+} can recover the oxidation activity of P-NCDs. Hence, efficient colorimetric Hg^{2+} detection with a linear range of 0.01–14 μM and a detection limit of 3.1 nM was achieved by detecting the color change of TMB. The feasibility of this strategy was validated through real sample analysis. Our study broadens the application scope of phosphorescent nanomaterials into colorimetric sensing.

© 2023 The Author(s). Published by Elsevier B.V. on behalf of King Saud University. This is an open access article under the CC BY-NC-ND license (<http://creativecommons.org/licenses/by-nc-nd/4.0/>).

1. Introduction

Nanozymes are a type of nanomaterials with similar properties as natural enzymes. Compared with natural enzymes, nanozymes have lower costs, higher stability, efficient and adjustable activities, and large-scale production (Bilal et al., 2023; Ouyang et al., 2022; Wu et al., 2019; Zhang et al., 2022). Hence, nanozymes are widely used to mimic various enzymes, such as peroxidase, oxidase, catalase, and superoxide dismutase (Lopez-Cantu et al., 2022; Wu et al., 2019; Zhang et al., 2022). Among them, peroxidase-like nanomaterials can catalyze the oxidation substrate of H_2O_2 to induce absorbance changes or fluorescent signals and thus are widely used in sensing analysis

* Corresponding authors.

E-mail addresses: ZLF19646@163.com (L. Zhang), mym8207@126.com (Y. Miao).

Peer review under responsibility of King Saud University.



(Christus et al., 2018; Dong et al., 2021; Fan et al., 2021; Liu et al., 2021; Vázquez-González et al., 2017). However, the reaction system of such nanomaterials is relatively complex and will not help improve the analytical efficacy of sensors. In comparison, oxidase-like nanozymes need much simpler reaction conditions (e.g. the avoidance of H_2O_2) and thus are more promising in the field of sensing analysis (Lai et al., 2022; Li et al., 2018). Hence, novel simple and activity-controllable oxidase mimics developed for sensing analysis are of better application prospects.

Developing photoresponsive oxidase mimics is a very effective route (Du et al., 2018; Liu et al., 2019; Yuan et al., 2022; Zhang et al., 2021; Zhao et al., 2022; Zhao et al., 2021). Photoresponsive oxidase mimics, in a H_2O_2 -free environment, can photoactivate dissolved oxygen to generate reactive oxygen species (ROS), such as singlet oxygen (1O_2), superoxide free radicals ($O_2^{\cdot-}$), hydroxyl free radical ($\bullet OH$), and H_2O_2 (Liu et al., 2020; Zhang and Liu, 2020). Singlet oxygen is one major species of active oxygen, and is extensively used in photosensitization and photodynamic treatments owing to its efficient oxidation ability (Kearns, 1971; Scurlock et al., 1995; Wang et al., 2015). Thus, an efficient photosensitizer is needed to sensitize triplet ground-state molecular oxygen (3O_2 , spin forbidden) to singlet oxygen (1O_2) (Kovalev and Fujii, 2005; Schweitzer and Schmidt, 2003; Wang et al., 2016). However, most photosensitizers can generate 1O_2 only with the help of heavy atoms, such as iodine/bromine-containing organic dyes, transition metal compounds, and noble metal nanoparticles (Chen et al., 2017; Ma et al., 2016; Rey et al., 2017; Sun et al., 2013; Tavakkoli Yarakhi et al., 2022; Wu et al., 2013). The applications of these photosensitizers are limited by their high costs, photobleaching, and high biotoxicity. Thus, developing novel low-cost photosensitizers that can be easily synthesized is very urgent. Energy transfer easily occurs between 3O_2 and excited triplet (T_1) nanomaterials, forming 1O_2 (Plaetzer et al., 2009). Since room-temperature phosphorescence (RTP) is caused by the triplet excited state transition, photosensitive materials with high phosphorescent quantum yield are more favorable for 1O_2 generation.

Long-life RTP carbon dots (CDs) featured by high triplet excited state (T_1) quantum yield and long T_1 exciton lifetime are an ideal candidate of photosensitive oxygen activation owing to their high 1O_2 quantum yield, low costs, low toxicity, and high biocompatibility (Geng et al., 2022; Jia et al., 2021; Wang and Lu, 2022; Wang et al., 2022; Wei et al., 2021; Yang et al., 2023). Since energy transfer is achieved through intermolecular collision, the probability of collision and energy transfer between RTP CD photosensitizers, which have longer-life T_1 exciton (longer RTP life), and O_2 is higher, increasing the O_2 sensitivity of photosensitizers and the 1O_2 quantum yield. Hence, long-life RTP photosensitizers have higher 1O_2 yields (Gao et al., 2018a; Xu et al., 2020).

Herein, new long-life RTP nitrogen-doped carbon dots (P-NCDs) were synthesized from a one-step hydrothermal method with triethylenetetramine hexaacetic acid (TTHA) as the only raw material. Under UV lamp irradiation at 365 nm, the P-NCDs showed high oxidase-like activity, and catalytically oxidized the colorless 3,3',5,5'-tetramethylbenzidine (TMB) to a blue product (ox-TMB). On this basis, a rapid sensitive Hg^{2+} colorimetric sensor was designed (Fig. 1). When cysteine (Cys) existed in the TMB/P-NCDs system, Cys can block the generation of cation free radicals and reduce the blue ox-TMB to colorless TMB. When Hg^{2+} existed, its specific complexation with Cys recovered the oxidase-like activity of P-NCDs, which then oxidized TMB to blue ox-TMB again. Thus, this colorimetric sensing system can be used to rapidly detect Hg^{2+} .

2. Experimental section

2.1. Materials and instrumentations

The details of materials and instruments were shown in [Supporting Information](#).

2.2. Synthesis of P-NCDs

P-NCDs were synthesized hydrothermally. Into a beaker, first 0.79 g of TTHA and then 30 mL of ultrapure water were added and fully mixed under ultrasound. The miscible solution was transferred to a polytetrafluoroethylene reactor. Reaction proceeded in an air dry oven at 180 °C for 5 h, and then the system cooled down to room temperature. The resulting light yellow solution was filtrated through a microporous membrane (0.22 μm) and then dialyzed via a dialysis membrane (MWCO:1000 Da) for 24 h, with ultrapure water changed every 4 h. Finally, the solution in the dialysis membrane was collected and freeze-dried to form white solid products, which were exactly P-NCDs.

2.3. Photoresponsive oxidase-like activity of P-NCDs

The photoresponsive oxidase-like activity of P-NCDs was studied through direct oxidation of TMB. First, 50 μL of an acetic acid-sodium acetate (HAc-NaAc) buffer solution (0.2 M, pH 5.4), 100 μL of a TMB solution (10 mM), and 50 μL of the P-NCDs solution (20 mg/mL) were successively added to a cuvette, which was diluted to 1 mL with ultrapure water. Then the mixture was irradiated under a 365 nm UV lamp for 30 min (2 min on/2 min off). Finally, the oxidase-like activity of P-NCDs was investigated by detecting the absorbance at 652 nm. Each experiment was repeated three times.

2.4. Steady-state dynamics analysis of P-NCDs

The steady-state dynamics of P-NCDs were analyzed under the optimal conditions in a system containing 1 mg/mL P-NCDs, and the HAc-NaAc buffer solution (10 mM, pH 5.4) with different concentrations of TMB. Based on the dynamics data, the Michaelis-Menten parameter was calculated from the Lineweaver-Burk plots:

$$V = V_{max}[S]/(K_m + [S])$$

where V and $[S]$ are the initial velocity and TMB concentration respectively, K_m is the Michaelis-Menten constant, and V_{max} is the maximum reaction velocity.

2.5. Effects of scavenger type on catalytic activity of P-NCDs

To each sample solution, a specific species of active oxygen trapping agent was added to observe its effect on the activity of P-NCDs. The sample solutions were: HAc-NaAc buffer solution (10 mM, pH 5.4), P-NCDs (1 mg/mL), TMB (1 mM), and a specific trapping agent, such as mannitol (5 mM), tryptophane (2.5 mg/mL), catalase (200 U/mL), superoxide dismutase (300 U/mL) and ethanol (10 % vt). Then the mixed solutions were irradiated under a 365 nm UV lamp for different periods of time.

2.6. Colorimetric detection of Hg^{2+}

First, a Cys solution (60 μL , 400 μM) and Hg^{2+} solution of a specific concentration were added to 50 μL of an HAc-NaAc buffer solution (0.2 M, pH 5.4). The mixed solutions reacted

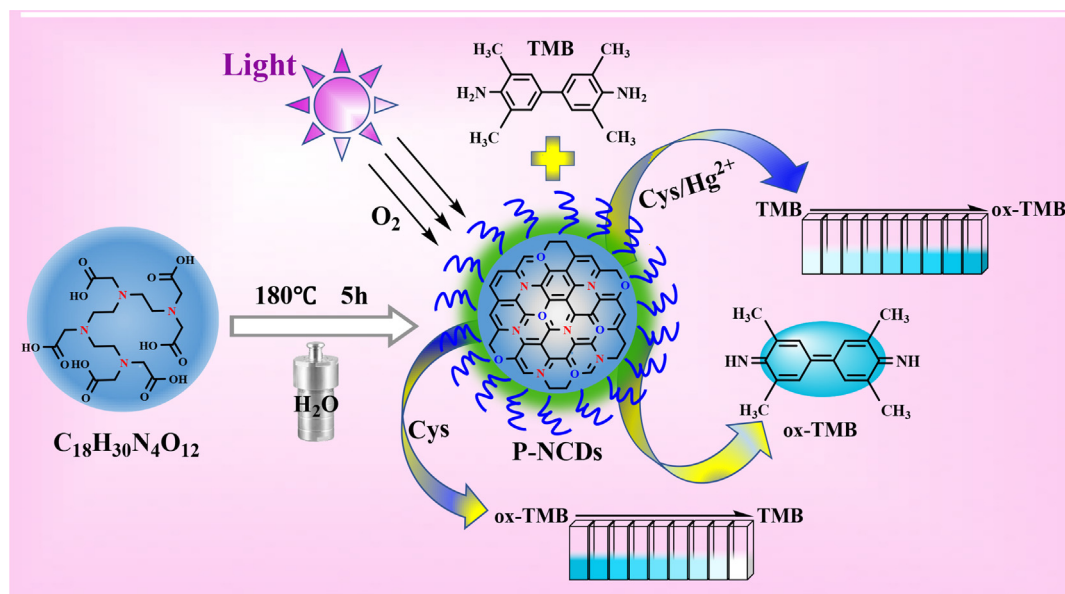


Fig. 1 Preparation and colorimetric Hg²⁺ detection of P-NCs.

at room temperature for 10 min. Then P-NCs (50 μ L, 20 mg/mL) and TMB (100 μ L, 10 mM) were added to each of the resulting mixtures above. Each mixed solution was diluted to 1 mL with ultrapure water and further reacted for 10 min. The resulting solutions were irradiated under the 365 nm UV lamp for 15 min, followed by observation of UV-vis spectra.

2.7. Analysis of real samples

Tap water (from our laboratory) and lake water (from a lake in our campus) were sampled and purified through 0.22 μ m microporous membranes. The resulting samples were used for analysis. Urine was collected from a healthy volunteer and diluted 100 times, without any other pretreatment.

3. Results and discussion

3.1. Synthesis and characterization of P-NCs

With TTHA as the only raw material, P-NCs with a dense core and some low-polymer long-chains on the surface were prepared via a one-step hydrothermal method (180 $^{\circ}$ C, 5 h), including high-temperature dehydration, condensation, crosslinking, and polymerization carbonization (Fig. 2A). The morphology and structure of the P-NCs were observed via TEM and XRD. The P-NCs are spherically shaped and evenly dispersed (Fig. 2B) in average grain diameter of \sim 3.2 5 nm (Fig. 2C) and without obvious lattice fringes, indicating the surface of P-NCs may have a polymer structure. The XRD patterns of P-NCs show an evident broad peak at 22 $^{\circ}$ (Fig. 2D), which further proves the existence of polymer carbon-dot and indicates the P-NCs have an amorphous structure. The hydrodynamic size of P-NCs was measured using dynamic light scattering (DLS) to be 90 nm (Fig. S1A), indicating the P-NCs have high water solubility. The hydration particle size of P-NCs is far larger than the particle size measured by TEM, which may be because the sur-

face low-polymer long chains of P-NCs are significantly hydrated and thereby extended. The zeta potential of P-NCs is 8.03 mV (Fig. S1B).

FTIR and XPS demonstrate the surface structure and chemical composition of P-NCs. The peak at 3442 cm^{-1} represents the surface O-H and N-H of P-NCs. The peaks at 3022, 1728, 1632, 1398, and 1224 cm^{-1} correspond to the stretching vibrations of C-H, COOH, C=C/C-N, C-O-C, and C-OH respectively (Fig. 2E). XPS further verifies the FTIR results. P-NCs show three characteristic peaks of C 1 s (286.0 eV), N 1 s (402.0 eV), and O 1 s (532.0 eV) (Fig. 2F). The high-resolution C 1 s spectrum splits into three peaks at 284.6, 285.9, and 288.2 eV (Fig. 2G), which correspond to C-C/C=C, C-N/C-O, and COOH, respectively. The high-resolution N 1 s spectrum shows two peaks at 399.3 and 401.5 eV (Fig. 2H), which stand for pyrrole nitrogen and N-H respectively. The O 1 s spectrum splits into two peaks at 531.2 and 533.1 eV (Fig. 2I), indicating the surface of P-NCs may contain C=O and C-OH. The above results indicate the surface of P-NCs is rich in O- and N-containing groups.

3.2. Optical properties and mechanism of P-NCs

During the irradiation under the 365 nm UV lamp, the P-NCs water solution emitted blue fluorescence (inset in Fig. 3A), without phosphorescence, and the fluorescence was excitation-dependent (Fig. S2A). The fluorescence attenuation curve was fitted using a double-exponential function, which showed the average lifetime was 7.17 ns (Fig. S2B). These photoinduced fluorescent properties indicate P-NCs may have multiple luminescence centers/channels. The absolute fluorescent quantum yield under excitation at 345 nm is 15.04 %.

The P-NCs powder were white in the environment, but emitted blue fluorescence under the ultraviolet lamp. After the ultraviolet radiation was stopped, the P-NCs powder showed obvious green RTP (inset in Fig. 3B). The offset of

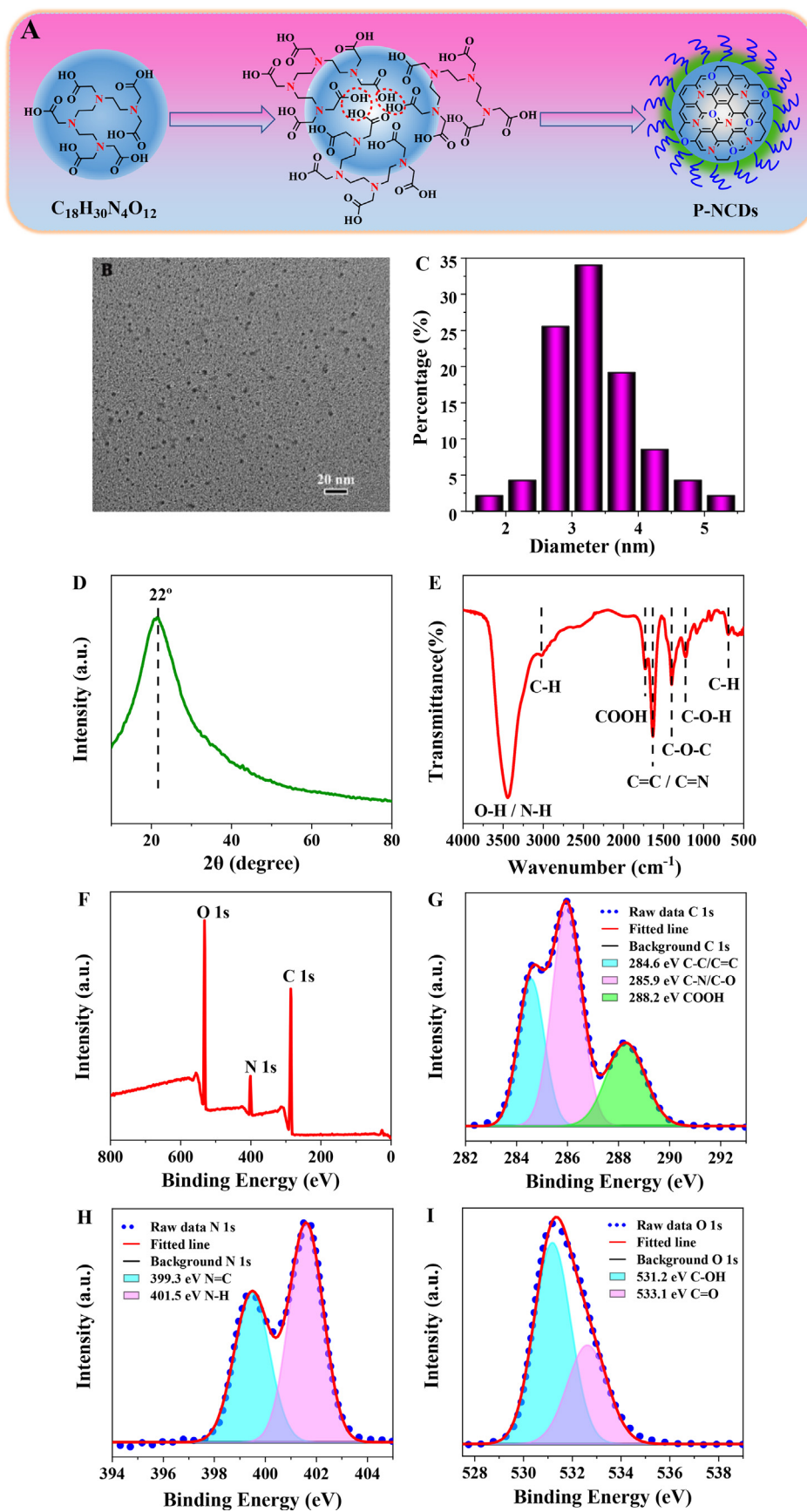


Fig. 2 (A) Schematic diagram about formation of P-NCs. Characterization of P-NCs: (B) TEM; (C) particle size distribution; (D) XRD spectra; (E) FT-IR spectra; (F) XPS spectra; (G) C 1s, (H) N 1s, (I) O 1s high-resolution spectra.

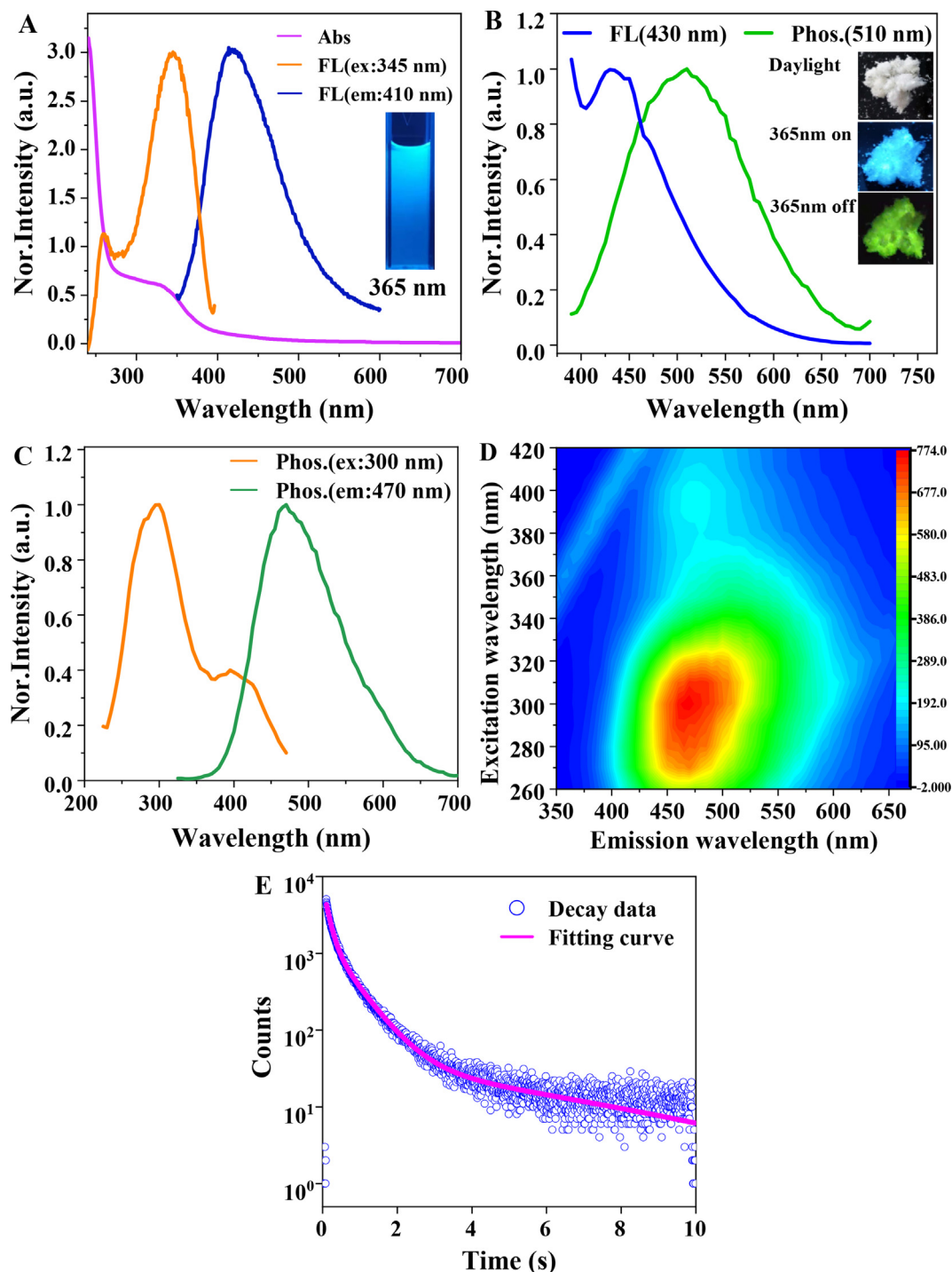


Fig. 3 (A) Normalized UV-vis spectrum (Abs), fluorescence (FL) optimal excitation and emission spectra of the P-NCDs solution. (B) fluorescence (FL) and phosphorescence (Phos.) spectra of P-NCDs powder under the 365 nm UV lamp. Inset: photos of P-NCDs powder in the environment with the 365 nm UV lamp on or off. (C) normalized optimal phosphorescence (Phos.) excitation and emission spectra of P-NCDs powder. (D) 3D phosphorescence spectrum of P-NCDs powder. (E) phosphorescence attenuation spectrum and fitted curve of P-NCDs powder.

the fluorescence from the phosphorescence emission center is 80 nm (Fig. 3B), indicating the energy gap between the singlet state and the triplet state is about 0.45 eV (Deng et al., 2013). In addition, the source of RTP emission from P-NCDs was studied according to the UV-vis and excitation spectra of P-

NCDs (Fig. 3A and 3C). The UV-vis absorption spectrum of P-NCDs shows wide bands at 275–400 nm, which may be ascribed to the $n-\pi^*$ transition of $C=O/C=N$ (Deng et al., 2013; Jiang et al., 2020; Li et al., 2016; Nie et al., 2021; Tao et al., 2018; Wu et al., 2022). The presence of $C=O/C=N$

can improve spin-orbit coupling and thereby promote intersystem crossing (ISC), forming more triplet-state excitons and producing RTP (Jiang et al., 2018b; Nie et al., 2021; Wang et al., 2021). The wider phosphorescent excitation band at 250–450 nm and the narrower fluorescent excitation band at 250–400 nm are largely overlapped with the absorption band of P-NCDs at 275–400 nm, indicating the fluorescent and phosphorescent emission of P-NCDs may come from the C=O/C=N of P-NCDs. Fig. 3D shows the 3D phosphorescence spectrum of P-NCDs powder. Compared with the fluorescence spectrum, the RTP emission evidently red-shifts. The P-NCDs powder also shows the excitation dependence as the P-NCDs solution. The phosphorescence attenuation spectrum of P-NCDs was fitted using a three-exponent function, and the lifetime was 140.07 ms (27.48 %), 627.21 ms (55.08 %) and 6086.33 ms (17.44 %) (Fig. 3E), suggesting the phosphorescence irradiation of P-NCDs originated from multiple luminescence centers. The average attenuation lifetime of P-NCDs was calculated to be 1.45 s.

Based on the above analyses, the RTP mechanism of P-NCDs can be predicted. First, the high-temperature dehydration, condensation, crosslinking and polymerized carbonization of triethylenetetramine hexaacetic acid form specific sub-fluorescent functional groups (C=O/C=N) responsible for phosphorescence emission, including the dense core and some low-polymer long-chains (Fig. 2A). The dense core and long chains of P-NCDs stably excite the triplet state and inhibit nonradiative transition, facilitating the phosphorescence emission of P-NCDs (Jiang et al., 2018a; Zhu et al., 2015). Then, TEM and XRD show the amorphous P-NCDs may contain a certain type of intertwined polymers, which act as the substrate to fix the luminescence center (Gao et al., 2020; Jiang et al., 2018b). FTIR and XPS demonstrate the surface of P-NCDs is rich in -OH and -COOH, which provide effective binding sites for forming the hydrogen bond and hydrogen bond frames of P-NCDs. These changes effectively prevent the triplet state excitons from being quenched by atmospheric water and oxygen and increase the probability of phosphorescent emission. In addition, TTHA, the only raw material, has both a carbon source and a doped nitrogen source. The introduction of N facilitates n- π^* transition and effectively promotes intersystem crossing, leading to an increase in effective triplet excitons and promoting phosphorescence emission (Gao et al., 2018b; Li et al., 2016). In all, the dense core, low-polymer long-chains, rigid hydrogen bonds, and nitrogen doping jointly promote the phosphorescent emission of P-NCDs.

3.3. Photoresponsive oxidase-like activity of P-NCDs

The photoresponsive oxidase-like activity of P-NCDs was studied with TMB as the coloration substrate. Under irradiation with the 365 nm UV lamp, the P-NCDs catalytically oxidized colorless TMB into blue TMB cation free radical (ox-TMB), and an intense peak appeared at 652 nm (Fig. 5A), which prove the oxidase-like activity of P-NCDs. In comparison, without P-NCDs or irradiation, no blue ox-TMB was formed, and no peak appeared. The above results confirm that P-NCDs have photoinduced oxidase-like activity. To make P-NCDs achieve the optimal oxidase activity and to maximize the Hg²⁺ colorimetric sensing performance, we studied the

effects of pH, P-NCDs concentration, TMB concentration, reaction temperature, and irradiation time on the catalytic activity of P-NCDs. Under irradiation, the absorbance of the pure TMB solution (curve a) first increased (the solution was obviously blue at pH 3.8–4.2) and then decreased (the solution did not change in color at pH 4.6–5.8) with the rise of pH (Fig. 4A). After P-NCDs were added to the TMB solution (curve b), the absorbance first rose and then dropped with the increment of pH. The difference of absorbance before and after the addition of P-NCDs (curve b-a) was calculated and found to be maximized at pH 5.4, and the solution before the addition of P-NCDs was colorless, indicating the errors due to coloration can be avoided at pH 5.4. The catalytic activity of P-NCDs was maximized at the concentration of 1.0 mg/mL (Fig. 4B) and at 35 °C (Fig. 4D). As the TMB concentration or irradiation time was increased, the catalytic activity of P-NCDs was further enhanced (Fig. 4C, E). After comprehensive consideration of detection sensitivity and analytical speed, we determined the optimal reaction conditions to be: room temperature, pH 5.4, 1 mg/mL P-NCDs, 1 mM TMB, 365 nm UV lamp irradiation for 15 min. Then the stability of P-NCDs was tested under the optimal conditions. Even after 60 days of storage, the P-NCDs still maintained high catalytic activity (Fig. S3).

When the lamp was repeatedly turned on or off, the oxidase-like activity of P-NCDs was enhanced in a ladder-like way (Fig. 5B), indicating P-NCDs have the optically controlled oxidase activity. The photocontrolled oxidase activity of P-NCDs was further studied via steady-state dynamics analysis. Fig. 5C shows the Michaelis-Menten curve and Lineweaver-Burk double-reciprocal curve (Fig. 5D). With the Lineweaver-Burk function, the Michaelis constant K_m and the maximum reaction velocity V_{max} were calculated to be 0.19 mM and 4.67×10^{-8} M s⁻¹ respectively. Compared with some natural enzymes and artificial enzymes, the K_m is lower and V_{max} is larger (Table S1), indicating P-NCDs as an oxidase mimic are more affinitive to and catalytically active over TMB.

3.4. Mechanism on oxidase-like activity of P-NCDs

As for the catalysis mechanism of P-NCDs, it is hypothesized that the photo-activated oxidase-like activity of P-NCDs is related to the produced singlet oxygen. To validate this mechanism, we conducted a series of experiments. First, compared with air-saturated solutions, the absorbance in the solution blown in with nitrogen for 1 min obviously decreased (Fig. 6A), indicating the dissolved oxygen in the solution was involved in the photoactivated oxidation. Then chemical scavengers were used to clarify the active oxygen produced from oxidation. Mannitol, catalase, superoxide dismutase, tryptophane, and ethanol were chosen to scavenge \bullet OH, H₂O₂, O₂⁻, ¹O₂, and h⁺ respectively. The oxidase-like activity was obviously weakened after the addition of tryptophane (Fig. 6B), indicating the photooxidation was mediated by ¹O₂. EPR further verifies the generation of ¹O₂ (Fig. 6C). The ¹O₂ producing ability of P-NCDs was assessed using 1,3-diphenylisobenzofuran (DPBF). As the irradiation time of the 365 nm UV lamp was extended, the absorbance at 418 nm of the P-NCDs and DPBF mixed solution gradually decreased (Fig. 6D). This result indicates the formation of active ¹O₂ in the reaction system.

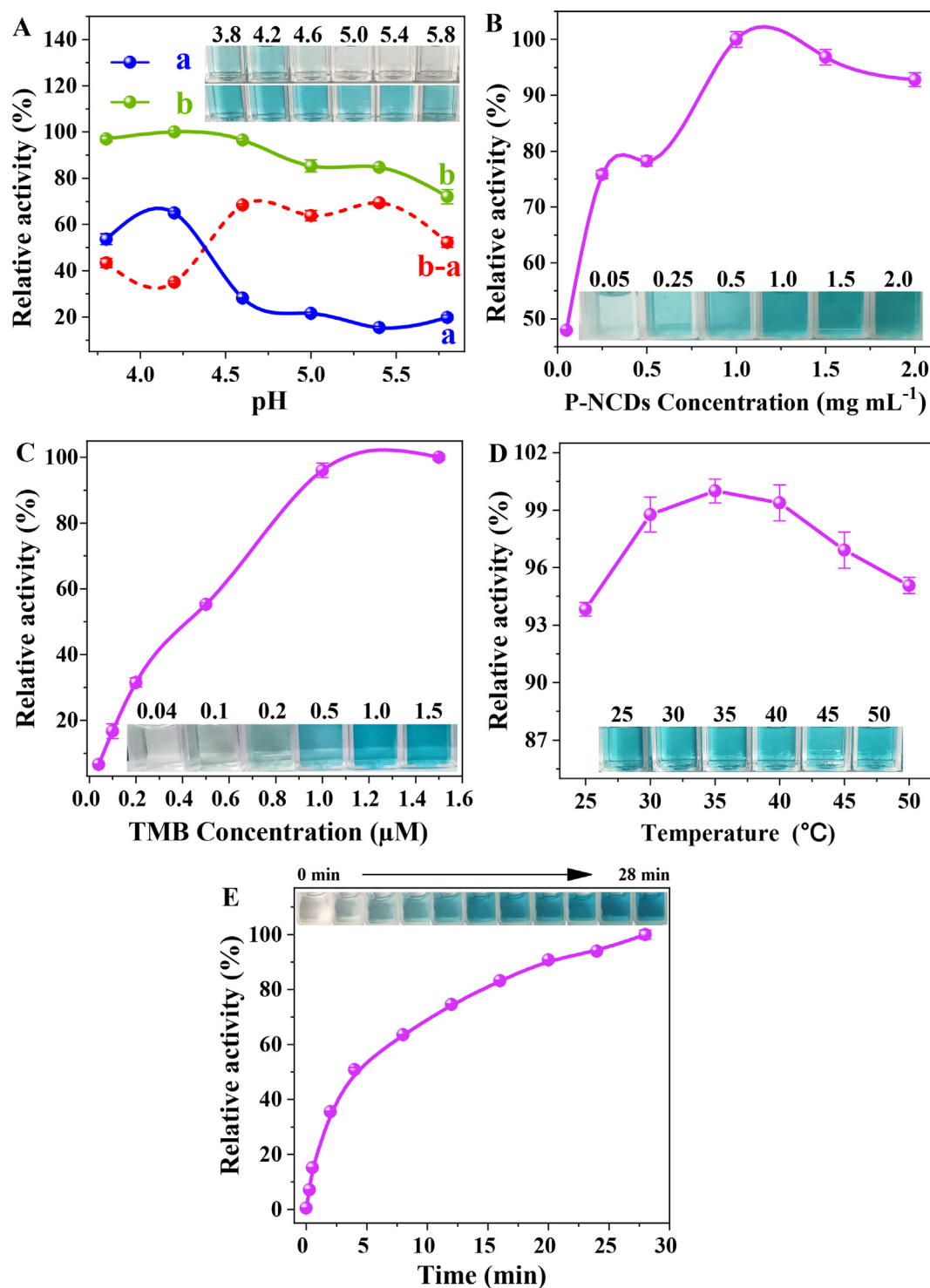


Fig. 4 Effects of (A) pH, a: TMB + Light, b: TMB + P-NCDs + Light; (B) P-NCDs concentration; (C) TMB concentration; (D) reaction temperature, and (E) irradiation time on catalytic activity of P-NCDs. Inset: photos of samples.

Based on the above results, we propose the mechanism underlying the photoinduced oxidase activity of P-NCDs (Fig. 6E): P-NCDs under ultraviolet illumination absorb photons, inducing electron transition from the ground state (S_0) to the excited singlet state (S_1). In addition to the fluorescence emission to recover the ground state in S_1 , the electrons of S_1 also can be transferred via intersystem crossing to the

excited triplet state (T_1) (Celli et al., 2010; Wang et al., 2016), so T_1 has longer lifetime than S_1 , and is attenuated via phosphorescence emission to the ground state. During the collision between the excited triplet-state P-NCDs and the triplet-state dissolved oxygen, energy was transferred to the surrounding oxygen molecules, forming 1O_2 (the scheme shown below) (DeRosa and Crutchley, 2002; Miao et al.,

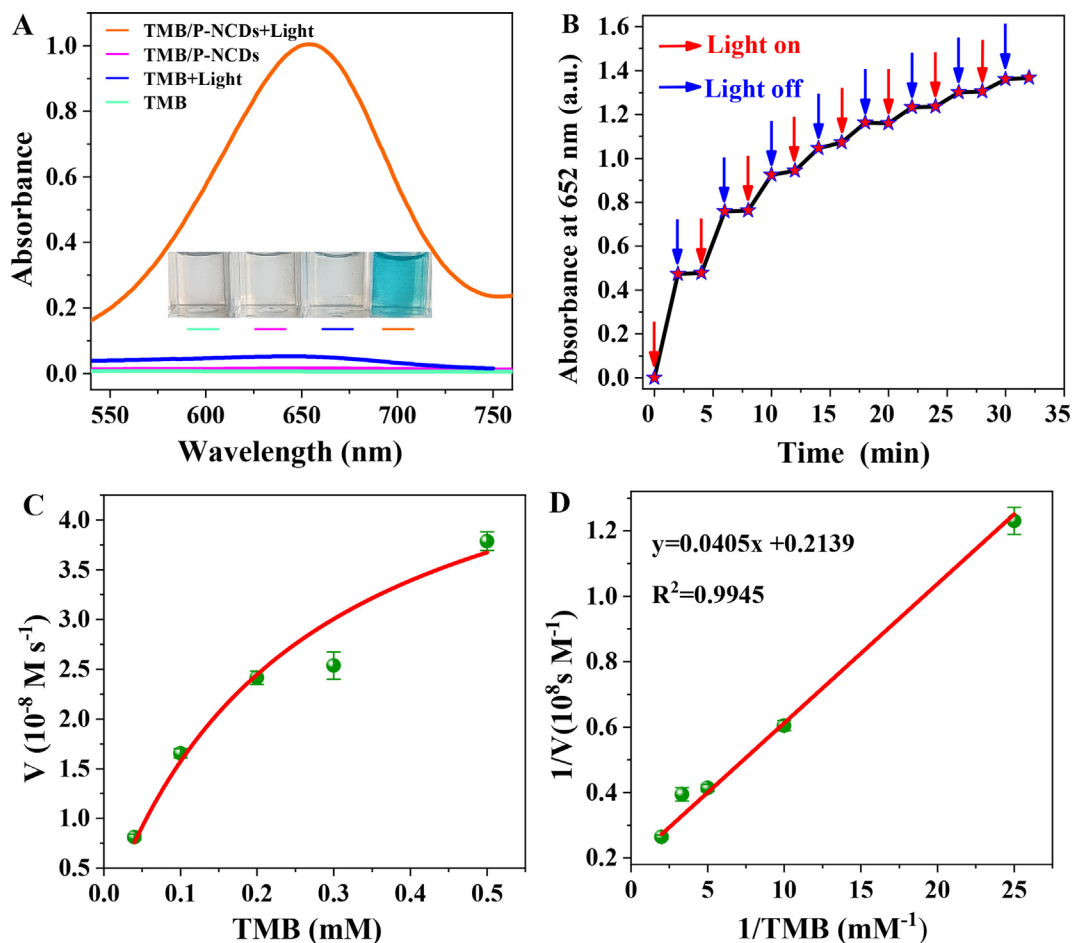
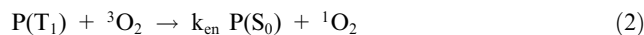
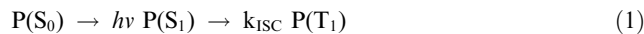


Fig. 5 (A) UV-vis spectra of samples under different conditions, including TMB/P-NCDs + Light, TMB/P-NCDs, TMB + Light, and TMB. Inset: photos of samples. (B) continuous on-and-off of the light source, and ladder-like behavior of oxidizing activity of P-NCDs. (C) Michaelis-Menten curve and (D) Lineweaver-Burk curve of catalytic activity of P-NCDs with TMB as the substrate.

2021; Plaetzer et al., 2009), which oxidized its substrate -- TMB to blue ox-TMB.



where P, photosensitizer; S_0 , singlet ground state, S_1 , the first excited singlet state; T_1 , the first excited triplet state; k_{ISC} , intersystem crossing rate constant; k_{en} , energy transfer rate constant; 3O_2 , ground-state triplet oxygen; 1O_2 , singlet oxygen.

3.5. Feasibility and mechanism of colorimetric Hg^{2+} detection

The experiments above prove the photoresponsive oxidase-like activity of P-NCDs, the ability to convert colorless TMB to blue ox-TMB, and the evident characteristic peaks (Fig. 5A). Fig. 7A illustrates the UV-vis spectra of three reaction systems. In the presence of Cys, the absorbance at 652 nm obviously decreased, and the solutions gradually turned from dark blue to light blue. In the coexistence of Cys and Hg^{2+} , the solutions became dark blue again, and the absorbance at 652 nm was recovered. The above results indicate this sensor is feasible for colorimetric detection of Hg^{2+} .

The mechanism of Hg^{2+} detection is shown in Fig. 7B. Under the 365 nm UV lamp irradiation, the P-NCDs photosensitized dissolved oxygen to form 1O_2 , which oxidized TMB to ox-TMB, so the solution turned blue. Cys added to the sensing system can prevent the formation of cation free radicals, so TMB cannot be converted to ox-TMB, 'turning off' the sensor and making the solution colorless. When Hg^{2+} existed in the sensing system, owing to its specific complexation with Cys, TMB can be converted to ox-TMB, 'turning on' the sensor and making the solution blue, which facilitated the colorimetric detection of Hg^{2+} .

3.6. Colorimetric detection of Hg^{2+}

As the Cys concentration rose, the absorption at 652 nm decreased (Fig. 7C). The reducible Cys effectively inhibited the TMB oxidation and color change by P-NCDs. Hence, the solution gradually turned from blue to light blue and even colorless (inset). The absorbance at 652 nm was linearly related to the Cys concentration (Fig. 7D). When Hg^{2+} existed, its specific complexation with Cys weakened the reducibility of Cys, so more colorless TMB was oxidized to blue ox-TMB. As the Hg^{2+} concentration rose, the absorbance intensity

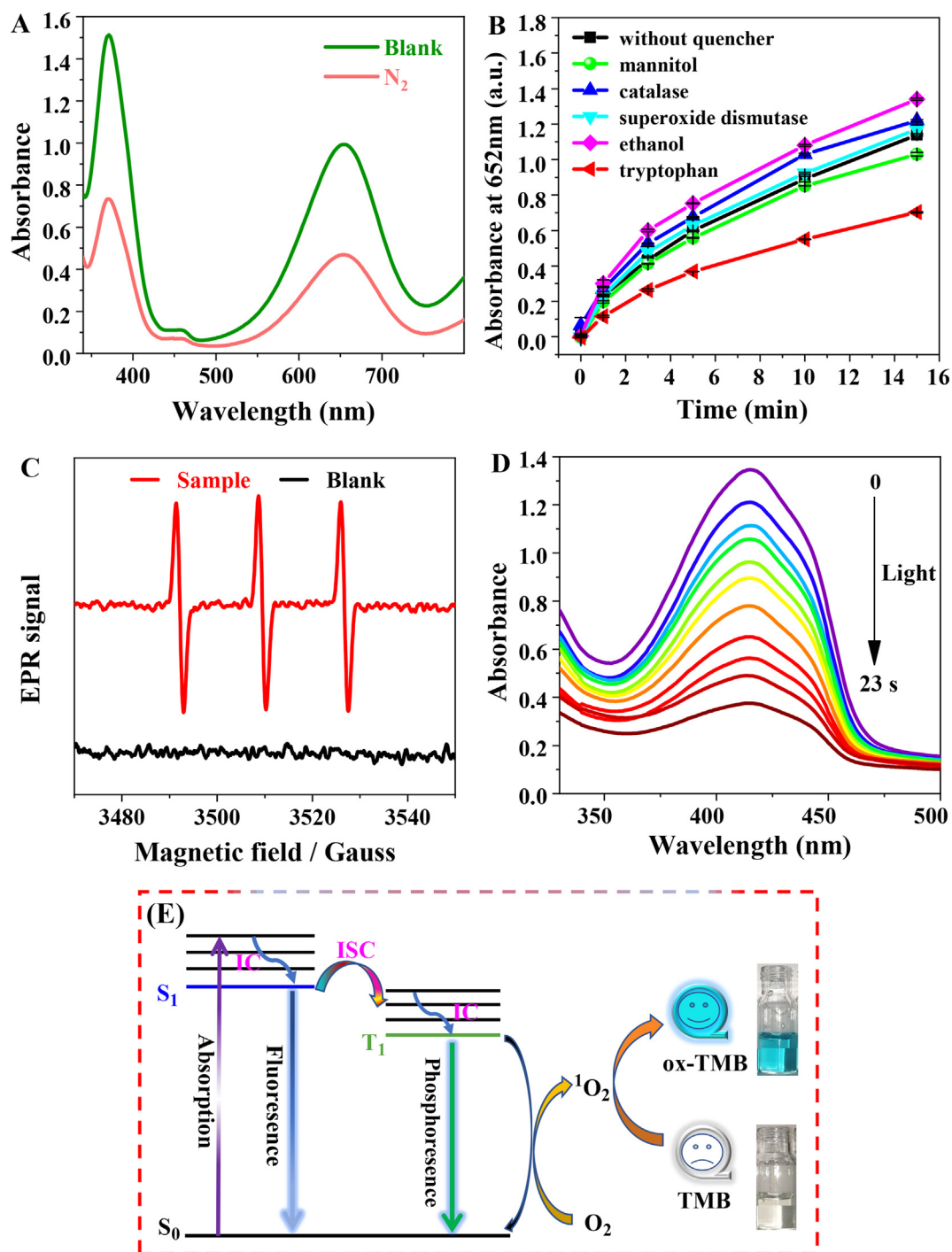


Fig. 6 (A) Effect of N_2 on oxidase-like activity of P-NCDs. (B) Effect of scavengers on TMB oxidation catalyzed by P-NCDs under 365 nm UV lamp irradiation. (C) EPR spectrum of P-NCDs (UV lamp irradiation time, 5 min) with the presence of TEMP (TEMP is a special spin trap of 1O_2). (D) absorption spectra of the P-NCDs (0.01 mg/mL) and DPBF (60 μ M) water mixed solutions after different duration of irradiation. (E) mechanism on the photoinduced oxidase activity of P-NCDs.

gradually increased (Fig. 7E), and the solution became dark blue (inset in Fig. 7F). The absorbance at 652 nm is well linearly related to the Hg^{2+} concentration, with a range of 0.01–14 μ M, $R_2 = 0.9933$ (Fig. 7F). The limit of detection (LOD) was calculated to be 3.1 nM ($LOD = 3\sigma/S$, where σ is the standard deviation of the absorbance of the blank sample ($n = 11$), and S is the slope of the standard curve). These results are similar to other Hg^{2+} detection methods (Table S2),

indicating this colorimetric sensor can rapidly and sensitively detect Hg^{2+} .

3.7. Selectivity in Hg^{2+} detection

To further assess the selectivity of the colorimetric sensor over specific metal ions, we studied its response to common metal ions. The effects of all metal ions on this sensor were low or

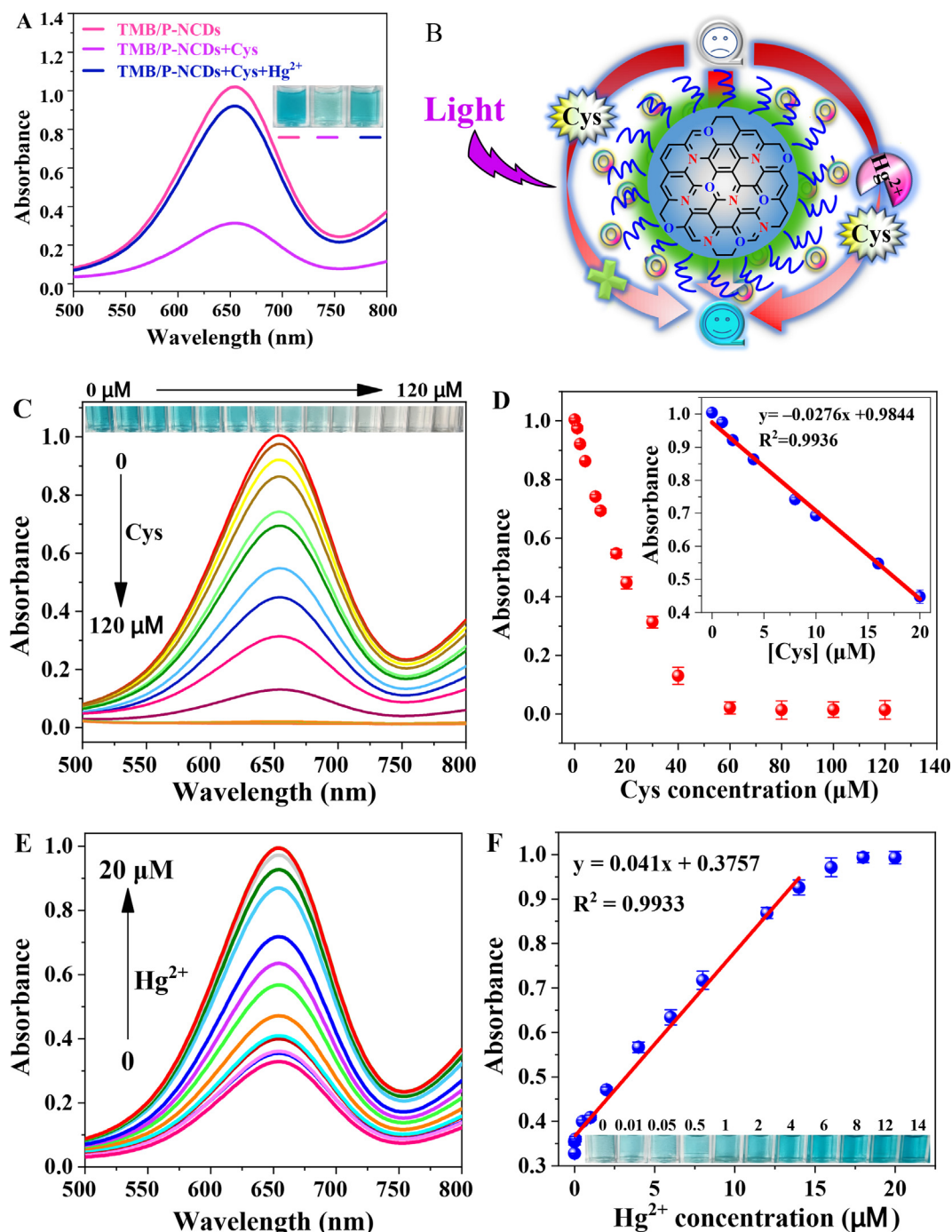


Fig. 7 (A) UV-vis spectra of TMB/P-NCDs, TMB/P-NCDs + Cys, and TMB/P-NCDs + Cys + Hg²⁺ systems under the 365 nm UV lamp. Inset: photos of samples. (B) mechanism of colorimetric Hg²⁺ detection. (C) UV-vis spectra of detection systems in response to different concentrations of Cys. Inset: relevant photos. (D) relationship between absorbance at 652 nm and Cys concentration. Inset: linear calibration curve of Cys detection. (E) UV-vis spectra of detection systems in response to different concentrations of Hg²⁺. (F) linear fitting between absorbance at 652 nm and Hg²⁺ concentration. Inset: photos of samples.

negligible (such as Na⁺, Mn²⁺, Ag⁺, Pb²⁺, Cr³⁺ only result in weak growth of absorbance, and some ions such as K⁺, Zn²⁺, Mg²⁺, Cd²⁺, Al³⁺, Ca²⁺, Ba²⁺, Ni²⁺ even caused a slight decrease in absorbance), except Cu²⁺ (Fig. S4A). The

significant enhancement of absorbance at 652 nm with the presence of Cu²⁺ may be ascribed to its high binding capacity. Hence, the potential interference from Cu²⁺ was eliminated (Fig. S4B). Then the ethylenediamine tetraacetic acid (EDTA)

and Cl^- mixture (molar ratio = 2: 1) was used as a masking agent (Lu et al., 2021), so the formation of a stable complex fully eliminated or avoided the interference from Cu^{2+} . In summary, this colorimetric sensor shows high selectivity in Hg^{2+} detection.

3.8. Analysis of real samples

To further explore whether this photoresponsive colorimetric sensing system was feasible for detecting Hg^{2+} in real samples, we conducted spiked recovery experiments by detecting Hg^{2+} in urine, tap water, and lake water. The spiked recovery rates are within 92.2 %-109.5 % (Table S3), suggesting this method can successfully detect Hg^{2+} in real samples.

4. Conclusions

Photoresponsive P-NCDs with oxidase-like activity were synthesized from a one-step hydrothermal method. Given the outstanding photoresponsive oxidase-like activity of P-NCDs, we designed a photo-stimulated colorimetric sensor that can detect Hg^{2+} by 'turning on and off' TMB molecules. Through the energy transfer from the excited triplet state to dissolved oxygen under irradiation by the 365 nm UV lamp, P-NCDs can produce singlet oxygen ($^1\text{O}_2$), which converts colorless TMB to blue ox-TMB. Cys prevented P-NCDs from oxidizing TMB, so the specific complexation between Hg^{2+} and Cys recovered the oxidase activity of P-NCDs, achieving the fast colorimetric detection of Hg^{2+} . Spiked recovery experiments suggest this method is feasible for detecting Hg^{2+} in real samples. This study offers a new strategy for Hg^{2+} monitoring in the environment and biological samples, and opens a new route for the sensing application of novel phosphorescent nanomaterials as model enzymes.

Declaration of Competing Interest

The authors declare that they have no known competing financial interests or personal relationships that could have appeared to influence the work reported in this paper.

Acknowledgments

This work was completed with the support of the National Natural Science Foundation of China (NSFC), China (32171393, 31700862), the Shanxi Postgraduate Education Innovation Project, China (2020BY083), and the Graduate Science and Technology Innovation Project of Shanxi Normal University, China (2019XBY014).

Author contributions

All authors contributed to literature research and manuscript writing.

Appendix A. Supplementary material

Supplementary data to this article can be found online at <https://doi.org/10.1016/j.arabjc.2023.104614>.

References

- Bilal, M., Khaliq, N., Ashraf, M., Hussain, N., Baqar, Z., Zdart, J., Jesionowski, T., Iqbal, H.M.N., 2023. Enzyme mimic nanomaterials as nanozymes with catalytic attributes. *Colloids Surf. B Biointerfaces* 221, 112950.
- Celli, J.P., Spring, B.Q., Rizvi, I., Evans, C.L., Samkoe, K.S., Verma, S., Pogue, B.W., Hasan, T., 2010. Imaging and photodynamic therapy: mechanisms, monitoring, and optimization. *Chem. Rev.* 110 (5), 2795–2838.
- Chen, Y.-Z., Wang, Z.U., Wang, H., Lu, J., Yu, S.-H., Jiang, H.-L., 2017. Singlet oxygen-engaged selective photo-oxidation over Pt nanocrystals/porphyrinic MOF: the roles of photothermal effect and Pt electronic state. *J. Am. Chem. Soc.* 139 (5), 2035–2044.
- Christus, A.A.B., Ravikumar, A., Panneerselvam, P., Radhakrishnan, K., 2018. A novel $\text{Hg}(\text{II})$ sensor based on $\text{Fe}_3\text{O}_4@ZnO$ nanocomposite as peroxidase mimics. *Appl. Surf. Sci.* 449, 669–676.
- Deng, Y., Zhao, D., Chen, X., Wang, F., Song, H., Shen, D., 2013. Long lifetime pure organic phosphorescence based on water soluble carbon dots. *Chem. Commun.* 49 (51), 5751–5753.
- DeRosa, M.C., Crutchley, R.J., 2002. Photosensitized singlet oxygen and its applications. *Coord. Chem. Rev.* 233–234, 351–371.
- Dong, L., Li, R., Wang, L., Lan, X., Sun, H., Zhao, Y., Wang, L., 2021. Green synthesis of platinum nanoclusters using lentinan for sensitively colorimetric detection of glucose. *Int. J. Biol. Macromol.* 172, 289–298.
- Du, J., Wang, J., Huang, W., Deng, Y., He, Y., 2018. Visible light-activatable oxidase mimic of 9-Mesityl-10-Methylacridinium ion for colorimetric detection of biothiols and logic operations. *Anal. Chem.* 90 (16), 9959–9965.
- Fan, L., Ji, X., Lin, G., Liu, K., Chen, S., Ma, G., Xue, W., Zhang, X., Wang, L., 2021. Green synthesis of stable platinum nanoclusters with enhanced peroxidase-like activity for sensitive detection of glucose and glutathione. *Microchem. J.* 166, 106202.
- Gao, Y., Han, H., Lu, W., Jiao, Y., Liu, Y., Gong, X., Xian, M., Shuang, S., Dong, C., 2018b. Matrix-free and highly efficient room-temperature phosphorescence of nitrogen-doped carbon dots. *Langmuir* 34 (43), 12845–12852.
- Gao, R., Mei, X., Yan, D., Liang, R., Wei, M., 2018a. Nano-photosensitizer based on layered double hydroxide and isophthalic acid for singlet oxygenation and photodynamic therapy. *Nat. Commun.* 9 (1), 2798.
- Gao, Y., Zhang, H., Shuang, S., Dong, C., 2020. Visible-light-excited ultralong-lifetime room temperature phosphorescence based on nitrogen-doped carbon dots for double anticounterfeiting. *Adv. Opt. Mater.* 8 (7), 1901557.
- Geng, B., Hu, J., Li, Y., Feng, S., Pan, D., Feng, L., Shen, L., 2022. Near-infrared phosphorescent carbon dots for sonodynamic precision tumor therapy. *Nat. Commun.* 13 (1), 5735.
- Jia, J., Lu, W., Gao, Y., Li, L., Dong, C., Shuang, S., 2021. Recent advances in synthesis and applications of room temperature phosphorescence carbon dots. *Talanta* 231, 122350.
- Jiang, K., Wang, Y., Cai, C., Lin, H., 2018a. Conversion of carbon dots from fluorescence to ultralong room-temperature phosphorescence by heating for security applications. *Adv. Mater.* 30 (26), 1800783.
- Jiang, K., Wang, Y., Gao, X., Cai, C., Lin, H., 2018b. Facile, quick, and gram-scale synthesis of ultralong-lifetime room-temperature-phosphorescent carbon dots by microwave irradiation. *Angew. Chem. Int. Ed.* 57 (21), 6216–6220.
- Jiang, K., Hu, S., Wang, Y., Li, Z., Lin, H., 2020. Photo-stimulated polychromatic room temperature phosphorescence of carbon dots. *Small* 16 (31), 2001909.

- Kearns, D.R., 1971. Physical and chemical properties of singlet molecular oxygen. *Chem. Rev.* 71 (4), 395–427.
- Kovalev, D., Fujii, M., 2005. Silicon nanocrystals: photosensitizers for oxygen molecules. *Adv. Mater.* 17 (21), 2531–2544.
- Lai, X., Shen, Y., Gao, S., Chen, Y., Cui, Y., Ning, D., Ji, X., Liu, Z., Wang, L., 2022. The Mn-modified porphyrin metal-organic framework with enhanced oxidase-like activity for sensitively colorimetric detection of glutathione. *Biosens. Bioelectron.* 213, 114446.
- Li, D., Liu, B., Huang, P.-J.-J., Zhang, Z., Liu, J., 2018. Highly active fluorogenic oxidase-mimicking NiO nanozymes. *Chem. Commun.* 54 (88), 12519–12522.
- Li, Q., Zhou, M., Yang, Q., Wu, Q., Shi, J., Gong, A., Yang, M., 2016. Efficient room-temperature phosphorescence from nitrogen-doped carbon dots in composite matrices. *Chem. Mater.* 28 (22), 8221–8227.
- Liu, Y., Wang, X., Wei, H., 2020. Light-responsive nanozymes for biosensing. *Analyst* 145 (13), 4388–4397.
- Liu, C., Zhang, M., Geng, H., Zhang, P., Zheng, Z., Zhou, Y., He, W., 2021. NIR enhanced peroxidase-like activity of Au@CeO₂ hybrid nanozyme by plasmon-induced hot electrons and photothermal effect for bacteria killing. *Appl. Catal. B Environ.* 295, 120317.
- Liu, Y., Zhou, M., Cao, W., Wang, X., Wang, Q., Li, S., Wei, H., 2019. Light-responsive metal-organic framework as an oxidase mimic for cellular glutathione detection. *Anal. Chem.* 91 (13), 8170–8175.
- Lopez-Cantu, D.O., González-González, R.B., Melchor-Martínez, E. M., Martínez, S.A.H., Araújo, R.G., Parra-Arroyo, L., Sosa-Hernández, J.E., Parra-Saldívar, R., Iqbal, H.M.N., 2022. Enzyme-mimicking capacities of carbon-dots nanozymes: properties, catalytic mechanism, and applications - a review. *Int. J. Biol. Macromol.* 194, 676–687.
- Lu, Z., Dang, Y., Dai, C., Zhang, Y., Zou, P., Du, H., Zhang, Y., Sun, M., Rao, H., Wang, Y., 2021. Hollow MnFeO oxide derived from MOF@MOF with multiple enzyme-like activities for multifunction colorimetric assay of biomolecules and Hg²⁺. *J. Hazard. Mater.* 403, 123979.
- Ma, Z., Zhang, M., Jia, X., Bai, J., Ruan, Y., Wang, C., Sun, X., Jiang, X., 2016. Fe^{III}-doped two-dimensional C₃N₄ nanofusiform: a new O₂-evolving and mitochondria-targeting photodynamic agent for MRI and enhanced antitumor therapy. *Small* 12 (39), 5477–5487.
- Miao, W., Zou, W.-S., Zhao, Q., Wang, Y., Chen, X., Wu, S., Liu, Z., Xu, T., 2021. Coupling room-temperature phosphorescence carbon dots onto active layer for highly efficient photodynamic antibacterial chemotherapy and enhanced membrane properties. *J. Membr. Sci.* 639, 119754.
- Nie, Y., Lai, W., Zheng, N., Weng, W., 2021. Multifunctional room-temperature phosphorescent carbon dots for relative humidity determination and information encryption. *Talanta* 233, 122541.
- Ouyang, Y., O'Hagan, M.P., Willner, I., 2022. Functional catalytic nanoparticles (nanozymes) for sensing. *Biosens. Bioelectron.* 218, 114768.
- Plaetzer, K., Krammer, B., Berlanda, J., Berr, F., Kiesslich, T., 2009. Photophysics and photochemistry of photodynamic therapy: fundamental aspects. *Lasers Med. Sci.* 24 (2), 259–268.
- Rey, Y.P., Abradelo, D.G., Santschi, N., Strassert, C.A., Gilmour, R., 2017. Quantitative profiling of the heavy-atom effect in BODIPY dyes: correlating initial rates, atomic numbers, and ¹O₂ quantum yields. *Eur. J. Org. Chem.* 2017 (15), 2170–2178.
- Schweitzer, C., Schmidt, R., 2003. Physical mechanisms of generation and deactivation of singlet oxygen. *Chem. Rev.* 103 (5), 1685–1758.
- Scurlock, R.D., Wang, B., Ogilby, P.R., Sheats, J.R., Clough, R.L., 1995. Singlet oxygen as a reactive intermediate in the photodegradation of an electroluminescent polymer. *J. Am. Chem. Soc.* 117 (41), 10194–10202.
- Sun, J., Zhong, F., Yi, X., Zhao, J., 2013. Efficient enhancement of the visible-light absorption of cyclometalated Ir(III) complexes triplet photosensitizers with bodipy and applications in photooxidation and triplet-triplet annihilation upconversion. *Inorg. Chem.* 52 (11), 6299–6310.
- Tao, S., Lu, S., Geng, Y., Zhu, S., Redfern, S.A.T., Song, Y., Feng, T., Xu, W., Yang, B., 2018. Design of metal-free polymer carbon dots: a new class of room-temperature phosphorescent materials. *Angew. Chem. Int. Ed.* 57 (9), 2393–2398.
- Tavakkoli Yarak, M., Liu, B., Tan, Y.N., 2022. Emerging strategies in enhancing singlet oxygen generation of nano-photosensitizers toward advanced phototherapy. *Nano-Micro Lett.* 14 (1), 123.
- Vázquez-González, M., Torrente-Rodríguez, R.M., Kozell, A., Liao, W.-C., Ceconello, A., Campuzano, S., Pingarrón, J.M., Willner, I., 2017. Mimicking peroxidase activities with prussian blue nanoparticles and their cyanometalate structural analogues. *Nano Lett.* 17 (8), 4958–4963.
- Wang, H., Jiang, S., Chen, S., Li, D., Zhang, X., Shao, W., Sun, X., Xie, J., Zhao, Z., Zhang, Q., Tian, Y., Xie, Y., 2016. Enhanced singlet oxygen generation in oxidized graphitic carbon nitride for organic synthesis. *Adv. Mater.* 28 (32), 6940–6945.
- Wang, B., Lu, S., 2022. The light of carbon dots: from mechanism to applications. *Matter* 5 (1), 110–149.
- Wang, Q., Pang, E., Tan, Q., Zhao, S., Yi, J., Zeng, J., Lan, M., 2022. Regulating photochemical properties of carbon dots for theranostic applications. *WIREs Nanomed. Nanobiotechnol.* p. e1862.
- Wang, H., Yang, X., Shao, W., Chen, S., Xie, J., Zhang, X., Wang, J., Xie, Y., 2015. Ultrathin black phosphorus nanosheets for efficient singlet oxygen generation. *J. Am. Chem. Soc.* 137 (35), 11376–11382.
- Wang, B., Yuan, X., Lv, X., Mei, Y., Peng, H., Li, L., Guo, Y., Du, J., Zheng, B., Xiao, D., 2021. Carbon dots-based room-temperature phosphorescent test strip: visual and convenient water detection in organic solvents. *Dyes Pigments* 189, 109226.
- Wei, X., Yang, J., Hu, L., Cao, Y., Lai, J., Cao, F., Gu, J., Cao, X., 2021. Recent advances in room temperature phosphorescent carbon dots: preparation, mechanism, and applications. *J. Mater. Chem. C* 9 (13), 4425–4443.
- Wu, W., Sun, J., Cui, X., Zhao, J., 2013. Observation of the room temperature phosphorescence of Bodipy in visible light-harvesting Ru(II) polyimine complexes and application as triplet photosensitizers for triplet-triplet-annihilation upconversion and photocatalytic oxidation. *J. Mater. Chem. C* 1 (30), 4577–4589.
- Wu, J., Wang, X., Wang, Q., Lou, Z., Li, S., Zhu, Y., Qin, L., Wei, H., 2019. Nanomaterials with enzyme-like characteristics (nanozymes): next-generation artificial enzymes (II). *Chem. Soc. Rev.* 48 (4), 1004–1076.
- Wu, Q., Wang, L., Yan, Y., Li, S., Yu, S., Wang, J., Huang, L., 2022. Chitosan-derived carbon dots with room-temperature phosphorescence and energy storage enhancement properties. *ACS Sustain. Chem. Eng.* 10 (9), 3027–3036.
- Xu, L., Zhou, K., Ma, H., Lv, A., Pei, D., Li, G., Zhang, Y., An, Z., Li, A., He, G., 2020. Ultralong organic phosphorescent nanocrystals with long-lived triplet excited states for afterglow imaging and photodynamic therapy. *ACS Appl. Mater. Interfaces* 12 (16), 18385–18394.
- Yang, L., Zhang, Q., Huang, Y., Luo, C., Quan, Z., Li, H., Sun, S., Xu, Y., 2023. A sequential dual-lock strategy for generation of room-temperature phosphorescence of boron doped carbon dots for dynamic anti-counterfeiting. *J. Colloid Interface Sci.* 632, 129–139.
- Yuan, M.Y., Xiao, S.J., Wu, Y.N., Qiu, A.T., Guo, J., Zhong, Z.Q., Zhang, L., 2022. Visual detection of captopril based on the light activated oxidase-mimic activity of covalent organic framework. *Microchem. J.* 175, 107080.
- Zhang, X., Chen, X., Zhao, Y., 2022. Nanozymes: versatile platforms for cancer diagnosis and therapy. *Nano-Micro Lett.* 14 (1), 95.
- Zhang, J., Liu, J., 2020. Light-activated nanozymes: catalytic mechanisms and applications. *Nanoscale* 12 (5), 2914–2923.

- Zhang, Y., Song, J., Shao, W., Li, J., 2021. Au@NH₂-MIL-125(Ti) heterostructure as light-responsive oxidase-like mimic for colorimetric sensing of cysteine. *Micropor. Mesopor. Mater.* 310, 110642.
- Zhao, J., Wang, H., Geng, H., Yang, Q., Tong, Y., He, W., 2021. Au/N-doped carbon dot nanozymes as light-controlled anti- and pro-oxidants. *ACS Appl. Nano Mater.* 4 (7), 7253–7263.
- Zhao, J., Gong, J., Wei, J., Yang, Q., Li, G., Tong, Y., He, W., 2022. Metal organic framework loaded fluorescent nitrogen-doped carbon nanozyme with light regulating redox ability for detection of ferric ion and glutathione. *J. Colloid Interface Sci.* 618, 11–21.
- Zhu, S., Song, Y., Shao, J., Zhao, X., Yang, B., 2015. Non-conjugated polymer dots with crosslink-enhanced emission in the absence of fluorophore units. *Angew. Chem. Int. Ed.* 54 (49), 14626–14637.